http://www.kidney-international.org

Cardiac remodeling and dysfunction in nephrotic syndrome

M Moreira-Rodrigues[1], R Roncon-Albuquerque Jr[2], T Henriques-Coelho[2], AP Lourenço[2], B Sampaio-Maia[1], J Santos[1], M Pestana[1] and AF Leite-Moreira[2]

[1]*Unit of Research and Development of Nephrology, University of Porto, Porto, Portugal and* [2]*Department of Physiology, Faculty of Medicine, University of Porto, Porto, Portugal*

There is an increased incidence of heart disease in patients with chronic nephrotic syndrome (NS), which may be attributable to the malnutrition and activated inflammatory state accompanying the sustained proteinuria. In this study, we evaluated renal function, cardiac morphometry, contractile function, and myocardial gene expression in the established puromycin aminonucleoside nephrosis rat model of NS. Two weeks after aminonucleoside injection, there was massive proteinuria, decreased creatinine clearance, and a negative sodium balance. Skeletal and cardiac muscle atrophy was present and was accompanied by impaired left ventricular (LV) hemodynamic function along with decreased contractile properties of isolated LV muscle strips. The expression of selected cytokines and proteins involved in calcium handling in myocardial tissue was evaluated by real time polymerase chain reaction. This revealed that the expression of interleukin-1β, tumor necrosis factor-α, and phospholamban were elevated, whereas that of cardiac sarco(endo)plasmic reticulum calcium pump protein was decreased. We suggest that protein wasting and systemic inflammatory activation during NS contribute to cardiac remodeling and dysfunction.

Kidney International (2007) **71,** 1240–1248; doi:10.1038/sj.ki.5002204; published online 25 April 2007

KEYWORDS: nephrotic syndrome; cardiovascular; renal function; proteinuria; cytokines

Correspondence: *AF Leite-Moreira, Faculty of Medicine of Porto – Department of Physiology, Al Prof. Hernâni Monteiro, Porto 4200-319, Portugal. E-mail: amoreira@med.up.pt*

Received 8 June 2006; revised 28 December 2006; accepted 23 January 2007; published online 25 April 2007

In the nephrotic syndrome (NS), massive proteinuria is accompanied by hypoproteinemia, protein wasting, and lean body mass reduction.[1–3] Anorexia and impaired intestinal absorption from the edematous gut are also contributory, inducing malnutrition.[4,5] Inflammatory activation, which frequently follows malnutrition, has been consistently reported in the NS. Plasma and urinary levels of tumor necrosis factor-α (TNF-α) are elevated in patients with NS[6,7] as well as the glomerular expression of TNF-α and interleukin-1β (IL-1β) in experimental models of NS.[8] In addition, treatment with TNF-α blocking agents ameliorates NS in both animal models and patients with corticosteroid-resistant NS.[9,10]

Proinflammatory cytokines, such as TNF-α, are major determinants of cachexia in several chronic diseases.[11,12] Circulating levels of TNF-α are elevated not only in the NS but also in patients with heart failure.[13,14] In the heart, TNF-α has a negative inotropic effect on cardiomyocytes[15,16] and its local overexpression in transgenic mice leads to progressive dilatation and failure.[17,18] Nevertheless, the increased incidence of heart disease in patients with chronic NS has been mainly attributed to coronary disease induced by dyslipidemia and hypercoagulability.[19,20] Recent evidences do not entirely support, however, this view. Serum lipids and lipoproteins are not significant predictors of endothelial dysfunction in patients with NS[21] and high cardiovascular mortality associated with proteinuria is not explained by the presence of classic cardiovascular risk factors such as hypertension or smoking.[19] In addition, a high incidence of unexplained cardiac disease has also been reported in children with focal segmental glomerulosclerosis.[22]

This study was undertaken in order to clarify the impact of protein wasting and inflammatory activation that accompany the NS on cardiac remodeling and myocardial function. Namely, we evaluated cardiac hemodynamics, contractile function of multicellular myocardial preparations, morphometric parameters, and myocardial gene expression of cytokines, growth factors, type B natriuretic peptide (BNP), myosin heavy-chain (MHC) isoforms, and calcium-handling genes in the well-established model of puromycin aminonucleoside (PAN)-induced NS.

RESULTS

Renal function, sodium balance, and sympathetic activity

PAN injection induced creatinine clearance reduction and massive proteinuria, present both 7 and 14 days after injection, whereas the disturbance of sodium handling was biphasic. On day 7, PAN-treated rats presented decreased fractional excretion of sodium (FE_{Na+}), positive sodium balance, and marked ascites, whereas on day 14 FE_{Na+} was increased, sodium balance was negative, and there was a reduction in ascites volume. Urinary noradrenaline was increased during the first 3 days after PAN injection and was decreased on days 7–9 after PAN injection (Table 1 and Figure 1).

Cardiac and skeletal muscle atrophy

On day 14, PAN-treated rats presented gastrocnemius and cardiac atrophy, with decreased organ weight to tibial length ratios and lower protein concentration to DNA concentration ratios. Gastrocnemius muscle atrophy was accompanied by decreased DNA content and cell size. Differently, cardiac atrophy was associated with increased cell size, but with no changes in DNA content. No significant fibrosis was detected in the myocardium of PAN-treated rats (Tables 1 and 2 and Figure 2).

Non-invasive blood pressure and cardiac hemodynamics

Non-invasive blood pressure recordings did not differ between the studied groups at both days 7 and 14. Heart rate was also similar between Control and PAN-treated rats 14 days after injection (414±9 and 389±26, respectively; beats/min) (Table 1).

PAN-treated rats presented basal hemodynamic recordings similar to Control rats and showed disturbed left ventricular (LV) systolic and diastolic function indexes only in isovolumetric (ISO) test heartbeats. Elevations of end-diastolic pressure (EDP) after an ISO cycle revealing diastolic intolerance to afterload (DIA) were already present 7 days after PAN injection, but most hemodynamic changes were apparent only 14 days after injection, with lower maximum pressure (P_{max}), peak rate of pressure rise (dP/dt_{max}), and absolute peak rate of pressure fall (dP/dt_{min}), and higher time constant τ, in ISO beats. Of note, hemodynamic disturbances were observed in the absence of significant differences in basal EDP and P_{max} (Table 3).

Contractile function of myocardial multicellular preparations

The contractile function of muscle strips from the LV myocardium was impaired 14 days after PAN injection. In fact, there was a significant reduction of both contractility and relaxation indexes, as evidenced by lower basal active tension (AT), peak isotonic shortening and maximum velocity of shortening (dL/dt_{max}), and lower absolute maximum velocity of lengthening (dL/dt_{min}), respectively. Trends toward decreased maximum velocity of tension rise (dT/dt_{max}) ($P=0.17$) and absolute maximum velocity of tension fall (dT/dt_{min}) ($P=0.06$) were also observed (Table 4).

The changes in AT in response to increasing stimulation frequencies were also distinct between Control and PAN-treated groups. The force–frequency relationship (FFR) was positive in the LV myocardium of Control rats, whereas in PAN group developed AT did not vary significantly with increasing stimulation frequencies (Figure 3).

Myocardial gene expression

LV gene expression of BNP, MHC, calcium-handling genes, and cytokines was altered after PAN injection, whereas no differences were observed for pre-pro-endothelin 1 and insulin-like growth factor 1 (IGF-1). BNP mRNA levels were

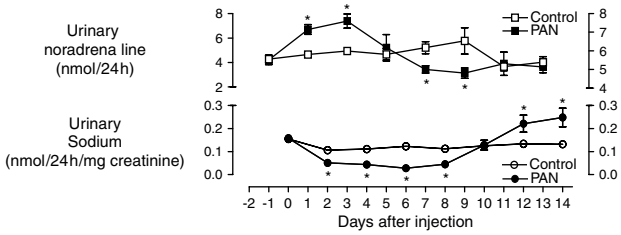

Figure 1 | Urinary excretion of sodium and urinary levels of noradrenaline in PAN and Control rats throughout the study. *$P<0.05$ vs Control rats.

Table 1 | Body weight, sodium balance, edema, renal function, and blood pressure in PAN nephrosis, 7 and 14 days after injection

	7 days		14 days	
	Control	PAN	Control	PAN
Body weight, g	221±5	248±4*	241±2	234±5
Na^+ balance, mmol/24 h	−0.03±0.07	0.90±0.07*	0.18±0.13	−0.61±0.38*
FE_{Na+}, %	0.14±0.01	0.04±0.01*	0.17±0.03	0.53±0.14*
Ascites, g	0.7±0.1	14.5±1.1*	0.6±0.1	1.3±0.3*
Creatinine clearance, ml/min	5.65±1.38	2.24±0.81*	4.51±1.08	2.24±0.32*
Urinary proteins, mg/24 h/mg creatinine	3.4±0.3	37.8±1.8*	3.8±0.7	51.0±9.0*
Systolic BP, mm Hg	155±8	147±6	138±4	150±7
Diastolic BP, mm Hg	106±9	86±8	86±3	86±7

BP, blood pressure; FE_{Na+}, fractional excretion of sodium; PAN, puromycin aminonucleoside.
Values are mean±s.e. of six experiments per group.
*$P<0.05$ vs Control rats.

Table 2 | Characterization of cardiac (LV) and skeletal muscle atrophy in PAN nephrosis, 7 and 14 days after injection

	7 days		14 days	
	Control	PAN	Control	PAN
Heart weight, mg	811.4±23.9	770.7±21.6	828.0±23.9	661.7±28.7*
Heart weight/tibial length, mg/mm	239.4±10.2	236.6±15.5	244.6±10.2	203.3±7.5*
LV weight/tibial length, mg/mm	169.4±6.5	166.9±11.5	174.2±6.6	144.4±5.6*
LV-$C_{protein}$/LV-C_{DNA}	96.0±3.7	96.6±3.5	96.2±3.0	69.8±4.4*
LV protein content, mg	20.8±0.9	21.8±1.1	21.5±0.9	14.9±0.8*
LV DNA content, mg	0.22±0.01	0.23±0.01	0.22±0.01	0.22±0.01
Gast weight/tibial length, mg/mm	408±5	374±26	458±11	206±52*
Gast-$C_{protein}$/Gast-C_{DNA}	229.2±20.0	224.3±16.7	226.9±20.1	161.1±19.8*
Gast protein content, mg	50.7±1.6	43.9±2.7	52.9±1.9	26.9±1.1*
Gast DNA content, mg	0.22±0.02	0.20±0.01	0.23±0.02	0.19±0.01*

C, concentration; Gast, gastrocnemius muscle; LV, left ventricle; PAN, puromycin aminonucleoside.
Values are mean±s.e. of six experiments per group.
*$P<0.05$ vs Control rats.

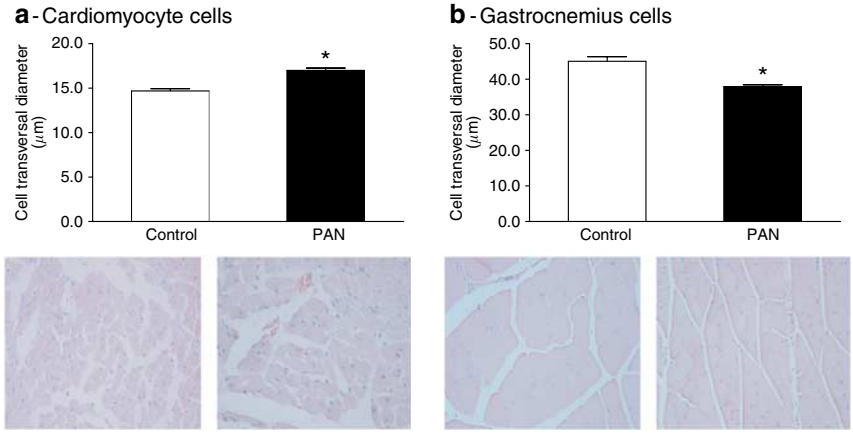

Figure 2 | Histology of the left ventricle (LV) and gastrocnemius muscle in PAN nephrosis, 14 days after injection. Cell transversal diameter of (**a**) cardiac (original magnification ×400 amplification, left ventricle) and (**b**) gastrocnemius muscle (original magnification ×200 amplification) cells, with respectively representative photographs. *$P<0.05$ vs control rats.

Table 3 | LV hemodynamics in PAN nephrosis, 7 and 14 days after injection

	Basal		ISO	
	Control	PAN	Control	PAN
7 days after injection				
EDP, mm Hg	1.6±0.8	3.1±0.1	2.6±0.3	3.6±0.4
P_{max}, mm Hg	102.1±9.6	101.0±10.9	190.2±22.4†	194.8±19.5†
dP/dt_{max}, mm Hg/s	4593±856	5189±627	5803±772	6368±558
dP/dt_{min}, mm Hg/s	−2907±591	−2921±462	−4285±650†	−4191±344†
Time constant τ, ms	23.3±2.8	22.2±0.6	21.2±2.5	20.7±1.7
DIA, mm Hg	—	—	0.2±0.1	1.7±0.6*
14 days after injection				
EDP, mm Hg	2.1±0.4	3.3±0.6	2.7±0.3	4.0±0.7
P_{max}, mm Hg	101.9±9.1	84.1±7.1	205.2±5.5†	164.8±14.2*†
dP/dt_{max}, mm Hg/s	4725±437	3411±501	5784±533	4012±398*
dP/dt_{min}, mm Hg/s	−2853±475	−2284±216	−4270±355†	−2717±404*
Time constant τ, ms	22.6±1.9	23.1±1.2	20.4±1.2	33.7±3.2*†
DIA, mm Hg	—	—	0.2±0.2	1.9±0.4*

DIA, diastolic intolerance to afterload; dP/dt_{max} and dP/dt_{min}, peak rates of pressure rise and fall, respectively; EDP, end-diastolic pressure; ISO, isovolumetric test heartbeat; LV, left ventricle; PAN, puromycin aminonucleoside; P_{max}, maximum pressure.
Values are mean±s.e. of six experiments per group.
*$P<0.05$ vs Control rats; $^{\dagger}P<0.05$ vs basal heartbeat.

Table 4 | Contractile parameters of myocardial (LV) multicellular muscle preparations in PAN nephrosis, at basal stimulation frequency (0.5 Hz), 14 days after injection

	Control	PAN
AT, mN/mm^2	0.80 ± 0.30	0.22 ± 0.08*
dT/dt_{max}, mN/mm^2/s	11.2 ± 5.0	4.0 ± 1.7
dT/dt_{min}, mN/mm^2/s	−14.1 ± 5.3	−4.1 ± 1.7
tHR, ms	116.9 ± 9.4	117.4 ± 1.0
PS, %L_{max}	5.00 ± 1.65	0.51 ± 0.23*
dL/dt_{max}, L_{max}/s	1.07 ± 0.35	0.11 ± 0.05*
dL/dt_{min}, L_{max}/s	−1.02 ± 0.36	−0.07 ± 0.03*
tdL/dt_{min}, ms	114.0 ± 10.5	119.2 ± 4.6

AT, active tension; dL/dt_{max} and dL/dt_{min}, maximum velocity of shortening and lengthening, respectively; dT/dt_{max}, and dT/dt_{min}, maximum velocity of tension rise and decline, respectively; L_{max}, maximum length; PS, peak isotonic shortening; tdL/dt_{min}, time to dL/dt_{min}; tHR, time to half relaxation.
Values are mean ± s.e. of six experiments per group.
*$P<0.05$ vs Control rats.

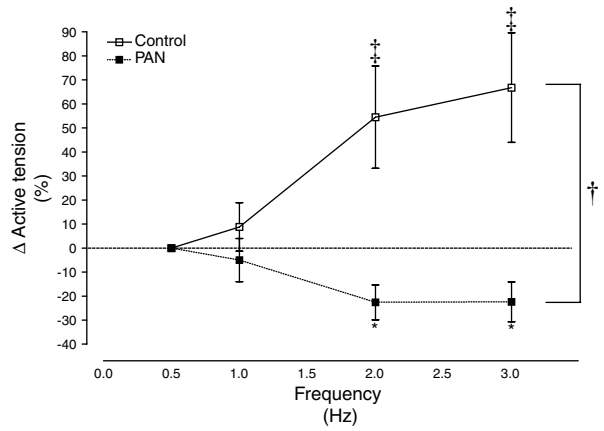

Figure 3 | FFRs obtained in multicellular muscle preparations from the LV myocardium in PAN nephrosis, 14 days after injection. Results are presented as percent variation from baseline AT at 0.5 Hz. †$P<0.05$ for interaction with two-way repeated measures analysis of variance; *$P<0.05$ vs Control rats at an equivalent frequency of stimulation; ‡$P<0.05$ vs 1 Hz, as evaluated with the Student–Newman–Keuls method for multiple group comparisons.

selectively elevated on day 7 in PAN-treated rats. MHC-α expression was also altered only on day 7, with decreased mRNA levels. Regarding calcium-handling genes, we detected sarcoplasmic reticulum calcium ATPase isoform 2a (SERCA2a) downregulation and phospholamban (PLB) upregulation 7 and 14 days after injection, whereas no significant differences were observed for Na^+/Ca^{2+} exchanger. Cytokine gene expression was also altered in PAN-treated rats: mRNA levels of TNF-α and IL-1β were upregulated, whereas no significant differences were observed for IL-6 and IL-1α (Figure 4).

Myocardial protein expression

Decreased myocardial LV SERCA2a protein levels were detected in PAN group, 14 days after injection, with no significant differences in PLB expression between Control and PAN groups. This resulted in a reduction of SERCA2a to PLB ratio in the PAN group (Figure 5).

DISCUSSION

PAN injection resulted in severe proteinuria and impaired creatinine clearance. As previously reported by others,[23] we found that the time course of variations of sodium retention and ascites accumulation in PAN nephrosis was divided into two phases. The first phase, from days 2 to 8, was marked by the decrease of sodium excretion accompanied with positive sodium balance and ascites accumulation. The second phase, from days 10 to 14, was marked by almost complete recovery of ascites, despite persistent high proteinuria. During this phase, urinary sodium excretion increased progressively toward higher than control levels from days 12 to 14, so that sodium balance was negative during this period. Most of the available evidence implicates a primary renal sodium handling abnormality in this edema formation condition.[24] In order to clarify the mechanisms underlying sodium balance regulation in PAN nephrosis, we studied sympathetic activity during the time span of the study. Interestingly, noradrenaline was reduced in 24 h urine during the second week after PAN injection, indicating that decreased sympathetic activity could contribute to negative sodium balance and increased FE_{Na+} from days 10 to 14.

Skeletal muscle atrophy, reduced gastrocnemius protein concentration to DNA concentration ratio, and reduced gastrocnemius cell size were observed in PAN-treated group on day 14. These findings agree well with previous observations in the passive Heymann nephritis model of NS, providing evidence for impaired muscle protein synthesis.[3] In our study, cardiac atrophy paralleled skeletal muscle atrophy in PAN-treated rats. This was not accompanied by LV decreased DNA content indicating that, LV cell death may not be present. Interestingly, the MHC-α gene, that codes a key component of the contractile apparatus and one of the most abundant proteins of cardiomyocytes, was downregulated on day 7 in PAN-injected rats, preceding cardiac atrophy. Although, to our knowledge, cardiac atrophy was never described in PAN nephrosis, van der Vijgh *et al.*[25] have previously shown morphometrically measurable cardiac abnormalities in PAN nephrosis 14 days after injection, namely an increase of the nuclear and reticulin indexes. Unloading is not a plausible explanation for cardiac atrophy, given the absence of significant differences in EDP between Control and PAN-injected rats. However, it should be noted that we did not assess LV volume and therefore could not rigorously assess LV preload. Although systolic and diastolic LV function was not significantly altered, impaired functional reserve was uncovered by hemodynamic stress with ISO beats. In fact, acute afterload elevations generating ISO cycles yielded lower dP/dt_{max} and P_{max}, decreased relaxation rate and increased diastolic intolerance to afterload in PAN-treated rats on day 14. The only hemodynamic disturbance present on day 7 was the elevation of diastolic intolerance to afterload after an ISO cycle, denoting diastolic intolerance to

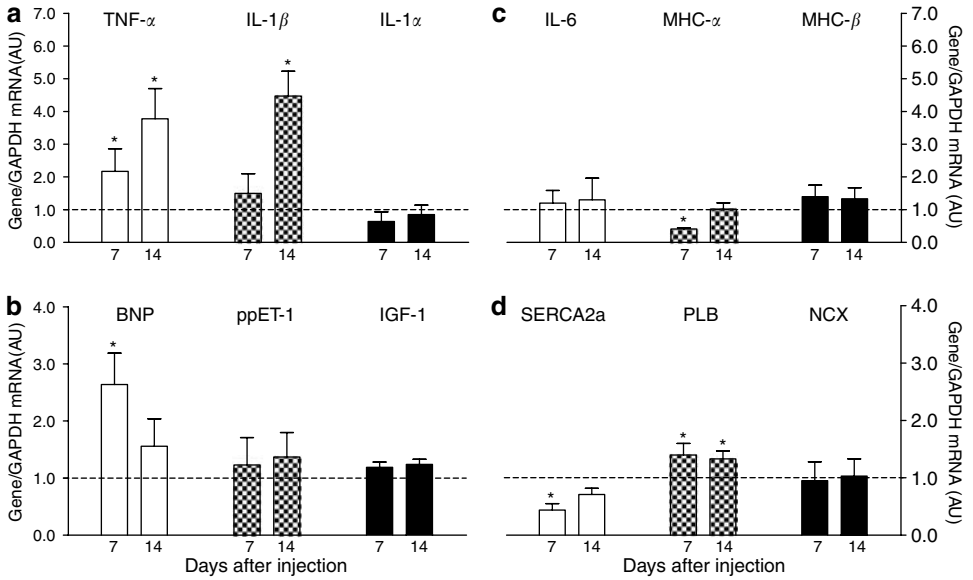

Figure 4 | LV mRNA expression in PAN nephrosis, 7 and 14 days after injection. The following genes were studied: (**a**) TNF-α, IL-1β, and IL-1α; (**b**) BNP, pre-pro-endothelin 1 (ppET-1), and IGF-1; (**c**) IL-6, MHC-α, and MHC-β and (**d**) SERCA2a, PLB, and Na^+/Ca^{2+} exchanger (NCX). Results are expressed as AUs after normalization for GAPDH. The AU was set as the average value of the Control group and is presented as a reference line. *$P<0.05$ vs Control rats.

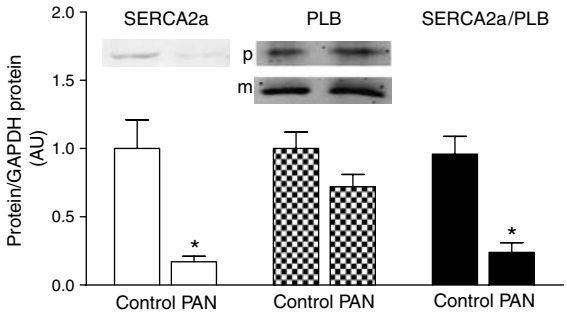

Figure 5 | LV protein levels of SERCA2a (110 kDa) and total PLB (pentamer 25 kDa plus monomer 10 kDa), with respectively representative immunoblots, and SERCA2a to PLB ratio in PAN nephrosis, 14 days after injection. Results are expressed as AUs after normalization for GAPDH protein. The AU was set as the average value of the Control group. p, PLB pentamer and m, PLB monomer. *$P<0.05$ vs Control rats.

acute afterload. We have previously proposed that this response to acute afterload elevations can be a precocious sign of dysfunction, preceding overt heart failure.[26]

To evaluate the intrinsic myocardial contractile function of PAN-treated rats, we used isolated multicellular preparations. Contractility, relaxation and FFRs were disturbed in the muscle strips of PAN-treated rats on day 14. Indeed, the positive FFR is an important intrinsic regulatory mechanism of cardiac contractility.[27] When it disappears or is inverted and becomes negative a central role is attributed to changes in calcium kinetic regulatory proteins such as SERCA2a.[27] Interestingly, we observed reduced levels of both SERCA2a mRNA and protein. Other authors have shown contractile function to be preserved on isolated papillary muscle experiments despite atrophic remodeling, 14 days after heterotopic heart transplantation.[28] These results suggest that mechanisms other than cardiac atrophy may contribute to myocardial dysfunction in PAN nephrosis.

In order to clarify the molecular mechanisms underlying cardiac remodeling, we evaluated both cardiac histology and myocardial gene expression. Regarding myocardial histology, we found increased cardiomyocyte diameter in the absence of significant fibrosis. This probably indicates enhanced cardiomyocyte edema, which could account for myocardial dysfunction. In fact, cardiac edema has been shown to increase myocardial stiffness and induce contractile dysfunction.[29] This has been attributed to increased myocardial expression of aquaporins.[29] Sympathetic activity is altered in PAN rats throughout the experiment, although the urinary levels of noradrenaline were similar between PAN and control rats on day 14. We cannot exclude that these changes in sympathetic activity may have influenced heart function throughout the study. Additionally, proinflammatory cytokines, TNF-α and IL-1β, were upregulated in the LV myocardium of PAN-treated rats. These results mimic the pattern of cytokine activation in the glomeruli of rats injected with PAN,[8] and might partly be explained taking in account that increased circulating levels of TNF-α were reported in the NS[6,7] and that TNF-α induces its own expression even in remote organs.[30] Local production of proinflammatory cytokines such as TNF-α in the heart is potentially relevant given its well-known effects in cardiac remodeling and contractile dysfunction.[13–16] Moreover, TNF-α is a major determinant of cachexia in several chronic diseases.[11,12] Disturbed cardiomyocyte calcium kinetics have also been implicated in the origin of myocardial dysfunction during heart failure progression.[26] In our study, cardiac atrophy was accompanied by decreased gene and protein expression of

SERCA2a, the main protein involved in calcium reuptake to the sarcoplasmic reticulum in the cardiomyocytes, and by increased mRNA levels and identical protein levels of its main inhibitor, PLB. The SERCA2a protein to PLB protein ratio was decreased. These results suggest that disturbed cardiomyocyte calcium kinetics could underlie myocardial dysfunction.

Although we did not evaluate the circulating levels of growth hormone and IGF-1, the absence of changes in LV IGF-1 mRNA levels in PAN-treated rats suggests that this pleitropic growth factor is not involved in cardiac remodeling. Nevertheless, we cannot exclude a systemic disturbance of the growth hormone/IGF-1 axis, as increased renal excretion and reduced circulating levels of IGF-1 and IGF-binding proteins have been reported in the NS.[31,32] This disturbance might contribute to growth and development retardation described both in experimental models and in children with poorly controlled NS.[5,33] We did not observe growth retardation, as estimated by tibial length, in PAN-treated rats. Still, the short time span of our study and the restriction of food ingestion in the Control group can explain this result. Given that anorexia contributes to the malnutrition observed in the NS, the control of food intake might have been particularly relevant.[34]

Elevated circulating levels of natriuretic peptides have been consistently observed in the NS.[35,36] Although the exact mechanisms underlying the activation of this natriuretic system are still unclear, myocardial stretch is unquestionably one of the main triggers for natriuretic peptide synthesis and release, both *in vitro* and *in vivo*.[37,38] In our study, we observed myocardial BNP overexpression in the initial phase of positive sodium balance and maximal edema (day 7). However, no significant changes in EDP or in blood pressure were present, suggesting absence of cardiac volume overload. These results support the observation that sodium retention, interstitial volume expansion, and edema formation are not uniformly accompanied by plasma volume expansion,[39] and suggest that factors other than myocardial stretch may stimulate natriuretic peptide system activation in the NS. In agreement with this latter view, proinflammatory cytokines, such as TNF-α and IL-1β, that have been shown to selectively upregulate BNP at the transcriptional and translational levels in cardiomyocytes,[40,41] were locally overexpressed in the heart of PAN-treated rats. Moreover, sodium renal loss and possible reduction of extracellular volume may explain why EDP was not elevated in the intact heart of PAN-injected rats at day 14 despite diastolic dysfunction, and may explain why myocardial BNP levels were upregulated at day 7, but not at day 14 after PAN injection.

Finally, the possibility that cardiac remodeling and contractile dysfunction could have resulted from direct cardiac effects of PAN must be addressed. PAN nephrosis is a commonly used and well-established experimental model of NS. Chemically, PAN is a nucleoside-like fragment structurally analogous to adenosine derived from puromycin by hydrolytic cleavage.[42] Although it shares some of the biological properties of puromycin, PAN is not a specific inhibitor of protein biosynthesis.[43–46] In fact, PAN does not inhibit *de novo* protein synthesis in either primary rat hepatocyte cultures[47] or rat thymocytes undergoing apoptosis.[48] Moreover, atrophy was not reported uniformly among organs in PAN nephrosis. Indeed, increased liver weight and hepatocyte protein synthesis have been demonstrated in this experimental model.[49] Furthermore, approximately 80% of PAN is excreted in the urine and feces within 24 h of administration in the rat, although most of the functional and structural changes were observed 14 days after injection.[50]

In conclusion, our results show that the proinflammatory state induced by PAN nephrosis involves the heart and is accompanied by cardiac remodeling and dysfunction. This might constitute a new mechanism underlying cardiac changes and cardiovascular risk in patients with NS.

MATERIALS AND METHODS

Animal experiments were performed according to the Portuguese law on animal welfare and conform to the National Institutes of Health Guide for the Care and Use of Laboratory Animals (NIH Pub. no. 85-23, Revised 1996). Normotensive male Sprague–Dawley rats ($n = 36$; Harlan, Interfauna Ibèrica, Barcelona, Spain), with a body weight of 200–220 g, were enrolled after a 7-day period of stabilization and adaptation to blood pressure measurements. The animals were kept under controlled environmental conditions (12:12 h light/dark cycle and $22 \pm 2^{\circ}$C room temperature).

Experimental model

The animals ($n = 6$ in each group) were studied 7 and 14 days after a single intraperitoneal injection of 150 mg/kg of PAN (Sigma-Aldrich, St Louis, MO, USA) or the same volume of vehicle (NaCl 0.9%). PAN-treated rats were fed *ad libitum* throughout the study with ordinary rat chow (0.19% sodium; Panlab, Barcelona, Spain). In order to control anorexia and sodium intake, the daily intake of rat chow in the Control group was limited to the intake of PAN group. Blood pressure and heart rate were measured using a photoelectric tail-cuff pulse detector (LE 5000, Letica, Barcelona, Spain) in conscious restrained animals. The animals were then placed in metabolic cages (Techniplast, Buguggiate, Italy) for 24 h urine collection. Finally, under anesthesia with sodium pentobarbital (50 mg/kg, intraperitoneal) LV hemodynamic parameters were assessed, blood was collected from the heart, morphometric measurements were performed, and LV samples were collected for molecular analysis. In an additional group of animals, the mechanical function of myocardial multicellular preparations was studied 14 days after injection of PAN ($n = 6$) or vehicle ($n = 6$).

Serum and urine biochemistry and edema formation

Quantification of sodium, creatinine, and total proteins was performed using Cobas Mira Plus analyzer (Horiba, ABX Diagnostics, Montpelier, France). Creatinine clearance, FE_{Na+}, and sodium balance were determined. Ascites volume was measured moistening and weighing an absorbent paper. Quantification of noradrenaline in urine was performed by high-performance liquid chromatography with electrochemical detection, as described previously.[51] In our laboratory, the lower limit of detection of noradrenaline ranged from 350 to 1000 fmol.

Morphometric analysis

The LV was weighted after dissecting the right ventricular free wall. Gastrocnemius muscle weight and tibial length were also measured.

Histology

Gastrocnemius and cardiac muscle sections (Microm STS HM340E, Walldorf, Germany), 4 μm thick, of paraffin-embedded formalin-fixed specimens were deparaffinized in xylene and rehydrated through graded ethanol. The sections were then stained with hematoxylin and eosin (Microm), and the smallest cardiomyocyte and gastrocnemius muscle cell transversal diameters were measured (Leica Application Suite Software, Leica Microsystems, Wetzlar, Germany). Collagen detection with Masson's trichrome staining (Bio-Optica, Milan, Italy) was performed to evaluate interstitial myocardial fibrosis.

Quantification of total protein and DNA concentration

Right gastrocnemius and LV samples were weighed ($\sim$12 mg), pulverized, and their protein and DNA concentration were determined. Protein quantification was performed after sample homogenization in a 4-(2-hydroxyethyl)-1-piperazineethanesulfonic acid (50 mM) buffer (150 KCl, 1.0 benzamidine, 0.1 EGTA, 1.0 PMSF, 1.0 DTT, and 0.1 CLAP; in mM), according to the Bradford method (Bio-Rad, Hercules, CA, USA) using bovine serum albumin as standard. Total DNA quantification was performed after sample homogenization and genomic DNA extraction (Bio-Rad) through ultraviolet spectrophotometry (Eppendorf, Hamburg, Germany). The DNA content was used as a surrogate of muscle cell number,[52] whereas the protein concentration to DNA concentration ratio was used as an index of cell size.[53]

Immunoblotting

LV free wall sample lysates were boiled in sample buffer (Bio-Rad) at 95°C for 5 min. Samples containing 40 μg of cell protein were separated by sodium dodecyl sulfate-polyacrylamide gel electrophoresis with 12% polyacrylamide gel and then electroblotted onto nitrocellulose membranes (Bio-Rad). Blots were blocked 1 h with 2% non-fat dry milk in Tris-buffered saline (50 mM Tris-HCl, 150 mM NaCl, pH 7,4) at room temperature with constant shaking. Blots were then incubated with anti-SERCA2a polyclonal antibody (1:200; Affinity Bioreagents, Golden, CO, USA) anti-PLB (1:2000, Cyclacel, Dundee, UK), and anti-glyceraldehyde-3-phosphate dehydrogenase (GAPDH) (1:2000; Abcam, Cambridge, UK) in 2% non-fat dry milk in Tris-buffered saline-T overnight at 4°C. The immunoblots were subsequently washed and incubated with fluorescently labeled goat anti-mouse secondary antibody (1:5000; AlexaFluor 680, Molecular Probes, Prat de Llobregat, Barcelona, Spain) or the fluorescently labeled goat anti-rabbit (1:10 000; IRDye™ 800, Rockland, PA, USA) for 60 min at room temperature and protected from light. The membrane was washed and imaged by scanning at both 800 and 700 nm, with an Odyssey Infrared Imaging System (LI-COR Biosciences, Lincoln, NE, USA).

Relative quantification of mRNA

Transmural LV free wall samples were collected, immersed in RNAlater (Qiagen, Hilden, Germany), and frozen (−80°C). Total mRNA was extracted through the guanidium thiocyanate selective silica-gel membrane-binding method (Qiagen), according to the manufacturer's instructions. Concentration and purity were assayed by spectrophotometry (Eppendorf). Two-step real-time reverse transcription-polymerase chain reaction (PCR) was used to perform relative quantification of mRNA. For each studied mRNA molecule, standard curves were generated from the correlation between the amount of starting total mRNA and PCR threshold cycle (second derivative maximum method) of graded dilutions from a randomly selected tissue sample ($r > 0.97$). For relative quantification of specific mRNA levels, 50 ng of total mRNA from each sample underwent two-step real-time reverse transcription-PCR. A melt curve analysis of each real-time PCR and 2% agarose gels (0.5 μg/ml ethidium bromide) was performed to exclude primer-dimer formation and assess the purity of the amplification product. GAPDH mRNA levels were similar in all experimental groups, which enabled the use of this gene as internal control. Results of mRNA quantification are expressed in an arbitrary unit (AU) set as the average value of the Control group (Control = 1 AU), after normalization for GAPDH. Reverse transcription (20 μl; 10 min at 22°C, 50 min at 50°C, and 10 min at 95°C) was performed in a standard thermocycler (Whatman Biometra, Goettingen, Germany): 40 U/reaction of reverse transcriptase (Invitrogen, Prat de Llobregat, Barcelona, Spain), 20 U/reaction of RNase inhibitor (Promega, WI, USA), 30 ng/ml random primers (Invitrogen), 0.5 mM nucleotide mix (MBI Fermentas, Corston Bath, UK), 1.9 mM $MgCl_2$, and 10 mM DTT. Ten percent of the cDNA yield was used as a template for real-time PCR (LightCycler, Roche, Indianapolis, IN, USA) using SYBR green (Qiagen), according to the manufacturer's instructions. Specific PCR primer pairs for the studied genes were as follows: **GAPDH** – forward (fw) 5′-TGG CCT TCC GTG TTC CTA CCC-3′ and reverse (rev) 5′-CCG CCT GCT TCA CCA CCT TCT-3′; **IGF-1** – fw 5′-CAG ACG GGC ATT GTG GAT-3′ and rev 5′-AGT CTT GGG CAT GTC AGT GTG-3′; **pre-pro-endothelin 1** – fw 5′-CCA TGC AGA AAG GCG TAA AAG-3′ and rev 5′-CGG GGC TCT GTA GTC AAT GTG-3′; **IL-1α** – fw 5′-GAG AGC CGG GTG GTG GTG TC-3′ and rev 5′-TCT GGG TTG GAT GGT CTC TTC TAA-3′; **IL-1β** – fw 5′-ATG GCA ACT GTC CCT GAA CTC-3′ and rev 5′-AAT CCT TAA TCT TTT GGG GTC TG-3′; **IL-6** – fw 5′-CCG TTT CTA CCT GGA GTT TG –3′ and rev 5′-GAA GTT GGG GTA GGA AGG AC-3′; **TNF-α** – fw 5′-GGG GGC CTC CAG AAC TCC A-3′ and rev 5′-TGG GCT ACG GGC TTG TCA-3′; **MHC-α** – fw 5′-CGA AGC GTG TCA TCC AGT-3′ and rev 5′-CTC CAG AGC AGG GTT AGC-3′; **MHC-β** – fw 5′-TGC TGA CAG ATC GGG AGA ACC-3′ and rev 5′-TGG CAG CAA TAA CAG CAA AAT-3′; **SERCA2a** – fw 5′-CGA GTT GAA CCT TCC CAC AA-3′ and rev 5′-GGA GGA GAT GAG GTA GCG GAT GGA-3′; **Na^+/Ca^{2+} exchanger** – fw 5′-CTG GAG CGC GAG GAA ATG TTA-3′ and rev 5′-GAC GGG GTT CTC CAA TCT CAA-3′; **PLB** – fw 5′-GGC ATC ATG GAA AAA GTC CA-3′ and rev 5′-GGT GGA GGG CCA GGT TGT AA-3′; **BNP** – fw 5′-GGA CCA AGG CCC TAC AAA AGA-3′ and rev 5′-CAG AGC TGG GGA AAG AAG AG-3′.

Hemodynamic studies

Animals were placed on a heated plate (body temperature 36–38°C) and the trachea was cannulated (Abocath® 16G) for mechanical ventilation (60 c.p.m.; tidal volume of 1 ml/100g; Harvard Small Animal Ventilator, Model 683) with oxygen-enriched air. Respiratory rate and tidal volume were adjusted to keep arterial blood gases and pH within physiological limits. The heart was then exposed through a median sternotomy and the pericardium widely opened. The ascending aorta was carefully dissected to allow its occlusion during the experimental protocol. LV pressures were measured with a 2-Fr high-fidelity micromanometer (SPR-324, Millar Instruments, Houston, TX, USA), inserted through the apex. After complete instrumentation, the animal preparation was allowed to stabilize for

15 min. Afterload elevations were performed by abrupt occlusion of the ascending aorta during diastole. The first heartbeat following constriction (ISO beat; ISO) was compared with the preceding basal heartbeat (Basal). These beat-to-beat interventions allow selective afterload elevation without neurohumoral activation, pericardial constraint, and preload or long-term load history changes.[54] After each occlusion, the animal was allowed to stabilize for several heartbeats. Hemodynamic recordings were made with ventilation suspended at end-expiration. Parameters were converted on-line to digital data with a sampling frequency of 1000 Hz. P_{max}, dP/dt_{max}, dP/dt_{min}, and EDP were measured. Relaxation rate was estimated with the time constant τ by fitting the ISO pressure fall to a mono-exponential function. Diastolic intolerance to acute afterload was assessed by computing the difference between EDP after and before an ISO cycle, as previously reported.[26]

Myocardial multicellular muscle preparations

Fourteen days after PAN or vehicle injection, rats were anesthetized and a left thoracotomy was performed. The beating heart was quickly excised and immersed in modified Krebs–Ringer solution containing (in mM) 93 NaCl, 5.0 KCl, 1.0 $MgSO_4$, 1.2 KH_2PO_4, 10 Glucose, 1.25 $CaCl_2$, 20 $NaHCO_3$, 1.0 NaH_2PO_4, 20 $Na_2H_3O_2$, 5 UI/l regular insulin with cardioplegic 2,3-butanedione monoxime (2.5%), equilibrated with a O_2/CO_2 mixture (95:5). Thin muscle strips were carefully isolated from LV papillary muscles under a dissecting microscope (Leica, Wilde M651), mounted horizontally in a 5-ml organ bath and attached to an electromagnetic length-tension transducer (University of Antwerp; Belgium). Twenty minutes later, bathing solutions were replaced by modified Krebs–Ringer solution without 2,3-butanedione monoxime. Preload was estimated according to muscle dimensions, and electrical stimulation was set 10% above threshold at a frequency of 0.5 Hz. Muscles were stabilized and the experimental protocol began once three comparable basal isotonic and isometric contractions were separately recorded with an interval of at least 10 min. Temperature was kept at 35°C and pH 7.35–7.45 throughout the experimental protocol. Isometric FFRs were obtained in PAN and Control by stepping up the frequency of stimulation at 3-min intervals and sequentially recording five contractions at 0.5 Hz, 1.0 Hz, 2.0 Hz, and 3.0 Hz. The analyzed parameters included AT, dT/dt_{max}, dT/dt_{min}, peak isotonic shortening, dL/dt_{max}, dL/dt_{min}, time to half relaxation, and time to dL/dt_{min} (tdL/dt_{min}). AT was computed from the weight and length of the muscle strip assuming an ellipsoidal shape. Muscle maximum cross-sectional diameters measured on a microscope (Leica) were similar in PAN (553 ± 108 μm) and Control (484 ± 77 μm).

Statistical analysis

Results are mean $\pm$ s.e. Repeated measures two-way analysis of variance followed by Student–Newman–Keuls method for multiple comparisons was applied to data from FFR in intact muscle strip preparations. On all other instances, comparisons were performed using Student's unpaired *t*-test; two-tailed values of $P < 0.05$ were considered statistically significant.

ACKNOWLEDGMENTS

This study was supported by a Grant from Sociedade Portuguesa de Nefrologia, and by grants POCI/SAU-OBS/55288/2004, POCI/SAU-MNO/61547/2004 and POCI/SAU-FCF/60803/2004 from Fundação para a Ciência e Tecnologia/FEDER. Mónica Moreira-Rodrigues was supported by Grant SFRH/BD/18869/2004 from Fundação para a Ciência e Tecnologia/FEDER.

REFERENCES

1. Cupisti A, Chisari C, Morelli E *et al.* Abnormal increase of creatine kinase plasma levels following muscle exercise in nephrotic patients. *Nephron* 1998; **80**: 204–207.
2. de Sain-Van Der Velden MG, de Meer K, Kulik W *et al.* Nephrotic proteinuria has no net effect on total body protein synthesis: measurements with (13)C valine. *Am J Kidney Dis* 2000; **35**: 1149–1154.
3. Kaysen GA, Carstensen A, Martin VI. Muscle protein synthesis is impaired in nephrotic rats. *Miner Electrolyte Metab* 1992; **18**: 228–232.
4. Maroni BJ, Staffeld C, Young VR *et al.* Mechanisms permitting nephrotic patients to achieve nitrogen equilibrium with a protein-restricted diet. *J Clin Invest* 1997; **99**: 2479–2487.
5. Thabet MA, Challa A, Chan W *et al.* Insulin-like growth factor and growth hormone receptor in nephrotic rats. *Am J Physiol* 1994; **266**: E102–E106.
6. Bustos C, Gonzalez E, Muley R *et al.* Increase of tumour necrosis factor alpha synthesis and gene expression in peripheral blood mononuclear cells of children with idiopathic nephrotic syndrome. *Eur J Clin Invest* 1994; **24**: 799–805.
7. Suranyi MG, Guasch A, Hall BM *et al.* Elevated levels of tumor necrosis factor-alpha in the nephrotic syndrome in humans. *Am J Kidney Dis* 1993; **21**: 251–259.
8. Gomez-Chiarri M, Ortiz A, Lerma JL *et al.* Involvement of tumor necrosis factor and platelet-activating factor in the pathogenesis of experimental nephrosis in rats. *Lab Invest* 1994; **70**: 449–459.
9. Martin A, Molina A, Bricio T *et al.* Passive dual immunization against tumour necrosis factor-alpha (TNF-alpha) and IL-1 beta maximally ameliorates acute aminonucleoside nephrosis. *Clin Exp Immunol* 1995; **99**: 283–288.
10. Raveh D, Shemesh O, Ashkenazi YJ *et al.* Tumor necrosis factor-alpha blocking agent as a treatment for nephrotic syndrome. *Pediatr Nephrol* 2004; **19**: 1281–1284.
11. Jackman RW, Kandarian SC. The molecular basis of skeletal muscle atrophy. *Am J Physiol Cell Physiol* 2004; **287**: C834–C843.
12. Moldawer LL, Copeland III EM. Proinflammatory cytokines, nutritional support, and the cachexia syndrome: interactions and therapeutic options. *Cancer* 1997; **79**: 1828–1839.
13. Testa M, Yeh M, Lee P *et al.* Circulating levels of cytokines and their endogenous modulators in patients with mild to severe congestive heart failure due to coronary artery disease or hypertension. *J Am Coll Cardiol* 1996; **28**: 964–971.
14. Torre-Amione G, Kapadia S, Lee J *et al.* Tumor necrosis factor-alpha and tumor necrosis factor receptors in the failing human heart. *Circulation* 1996; **93**: 704–711.
15. Torre-Amione G, Kapadia S, Lee J *et al.* Expression and functional significance of tumor necrosis factor receptors in human myocardium. *Circulation* 1995; **92**: 1487–1493.
16. Yokoyama T, Vaca L, Rossen RD *et al.* Cellular basis for the negative inotropic effects of tumor necrosis factor-alpha in the adult mammalian heart. *J Clin Invest* 1993; **92**: 2303–2312.
17. Li YY, Kadokami T, Wang P *et al.* MMP inhibition modulates TNF-alpha transgenic mouse phenotype early in the development of heart failure. *Am J Physiol Heart Circ Physiol* 2002; **282**: H983–H989.
18. Sivasubramanian N, Coker ML, Kurrelmeyer KM *et al.* Left ventricular remodeling in transgenic mice with cardiac restricted overexpression of tumor necrosis factor. *Circulation* 2001; **104**: 826–831.
19. Ordonez JD, Hiatt RA, Killebrew EJ *et al.* The increased risk of coronary heart disease associated with nephrotic syndrome. *Kidney Int* 1993; **44**: 638–642.
20. Watts GF, Herrmann S, Dogra GK *et al.* Vascular function of the peripheral circulation in patients with nephrosis. *Kidney Int* 2001; **60**: 182–189.
21. Dogra GK, Herrmann S, Irish AB *et al.* Insulin resistance, dyslipidaemia, inflammation and endothelial function in nephrotic syndrome. *Nephrol Dial Transplant* 2002; **17**: 2220–2225.
22. Adedoyin O, Frank R, Vento S *et al.* Cardiac disease in children with primary glomerular disorders-role of focal segmental glomerulosclerosis. *Pediatr Nephrol* 2004; **19**: 408–412.
23. Deschenes G, Doucet A. Collecting duct (Na+/K+)-ATPase activity is correlated with urinary sodium excretion in rat nephrotic syndromes. *J Am Soc Nephrol* 2000; **11**: 604–615.
24. Humphreys MH. Mechanisms and management of nephrotic edema. *Kidney Int* 1994; **45**: 266–281.

25. van der Vijgh WJ, Van Velzen D, Van der Poort JS *et al.* Morphometric study of myocardial changes during puromycin aminonucleoside induced nephropathy in rats. *Anticancer Res* 1987; **7**: 1111–1115.
26. Correia Pinto J, Henriques-Coelho T, Roncon-Albuquerque Jr R *et al.* Differential right and left ventricular diastolic tolerance to acute afterload and NCX gene expression in Wistar rats. *Physiol Res* 2006; **55**: 513–526.
27. Endoh M. Force–frequency relationship in intact mammalian ventricular myocardium: physiological and pathophysiological relevance. *Eur J Pharmacol* 2004; **500**: 73–86.
28. Welsh DC, Dipla K, McNulty PH *et al.* Preserved contractile function despite atrophic remodeling in unloaded rat hearts. *Am J Physiol Heart Circ Physiol* 2001; **281**: H1131–H1136.
29. Egan JR, Butler TL, Au CG *et al.* Myocardial water handling and the role of aquaporins. *Biochim Biophys Acta* 2006; **1758**: 1043–1052.
30. Nakamura H, Umemoto S, Naik G *et al.* Induction of left ventricular remodeling and dysfunction in the recipient heart after donor heart myocardial infarction: new insights into the pathologic role of tumor necrosis factor-alpha from a novel heterotopic transplant-coronary ligation rat model. *J Am Coll Cardiol* 2003; **42**: 173–181.
31. Haffner D, Tonshoff B, Blum WF *et al.* Insulin-like growth factors (IGFs) and IGF binding proteins, serum acid-labile subunit and growth hormone binding protein in nephrotic children. *Kidney Int* 1997; **52**: 802–810.
32. Lee DY, Park SK, Kim JS. Insulin-like growth factor-I (IGF-I) and IGF-binding proteins in children with nephrotic syndrome. *J Clin Endocrinol Metab* 1996; **81**: 1856–1860.
33. Zhou X, Loke KY, Pillai CC *et al.* IGFs and IGF-binding proteins in short children with steroid-dependent nephrotic syndrome on chronic glucocorticoids: changes with 1 year exogenous GH. *Eur J Endocrinol* 2001; **144**: 237–243.
34. Dong F, Ren J. Insulin-like growth factors (IGFs) and IGF-binding proteins in nephrotic syndrome children on glucocorticoid. *Pharmacol Res* 2003; **48**: 319–323.
35. Pedersen EB, Danielsen H, Eiskjaer H *et al.* Increased atrial natriuretic peptide in the nephrotic syndrome. Relationship to the renal function and the renin–angiotensin–aldosterone system. *Scand J Clin Lab Invest* 1988; **48**: 141–147.
36. Plum J, Mirzaian Y, Grabensee B. Atrial natriuretic peptide, sodium retention, and proteinuria in nephrotic syndrome. *Nephrol Dial Transplant* 1996; **11**: 1034–1042.
37. Pikkarainen S, Tokola H, Kerkela R *et al.* Endothelin-1-specific activation of B-type natriuretic peptide gene via p38 mitogen-activated protein kinase and nuclear ETS factors. *J Biol Chem* 2003; **278**: 3969–3975.
38. van Wamel JE, Ruwhof C, van der Valk-Kokshoorn EJ *et al.* Rapid gene transcription induced by stretch in cardiac myocytes and fibroblasts and their paracrine influence on stationary myocytes and fibroblasts. *Pflugers Arch* 2000; **439**: 781–788.
39. Perico N, Remuzzi G. Renal handling of sodium in the nephrotic syndrome. *Am J Nephrol* 1993; **13**: 413–421.
40. He Q, LaPointe MC. Interleukin-1beta regulation of the human brain natriuretic peptide promoter involves Ras-, Rac-, and p38 kinase-dependent pathways in cardiac myocytes. *Hypertension* 1999; **33**: 283–289.
41. Ma KK, Ogawa T, de Bold AJ. Selective upregulation of cardiac brain natriuretic peptide at the transcriptional and translational levels by pro-inflammatory cytokines and by conditioned medium derived from mixed lymphocyte reactions via p38 MAP kinase. *J Mol Cell Cardiol* 2004; **36**: 505–513.
42. Studzinski GP, Ellem KA. Relationship between RNA synthesis, cell division, and morphology of mammalian cells. I. Puromycin aminonucleoside as an inhibitor of RNA synthesis and division in HeLa cells. *J Cell Biol* 1966; **29**: 411–421.
43. Allen DW, Zamecnik PC. The effect of puromycin on rabbit reticulocyte ribosomes. *Biochim Biophys Acta* 1962; **55**: 865–874.
44. Hofert JF, Boutwell RK. Puromycin-induced glycogenolysis as an even independent from inhibited protein synthesis in mouse liver; effects of puromycin analogs. *Arch Biochem Biophys* 1963; **103**: 338–344.
45. Nathans D, Neidle A. Structural requirements for puromycin inhibition of protein synthesis. *Nature* 1963; **197**: 1076–1077.
46. Rabinovitz M, Fisher JM. A dissociative effect of puromycin on the pathway of protein synthesis by Ehrlich ascites tumor cells. *J Biol Chem* 1962; **237**: 477–481.
47. Sidhu JS, Omiecinski CJ. Protein synthesis inhibitors exhibit a nonspecific effect on phenobarbital-inducible cytochrome *P*450 gene expression in primary rat hepatocytes. *J Biol Chem* 1998; **273**: 4769–4775.
48. Chow SC, Peters I, Orrenius S. Reevaluation of the role of *de novo* protein synthesis in rat thymocyte apoptosis. *Exp Cell Res* 1995; **216**: 149–159.
49. Kawashima A, Chiku K, Kawashima M *et al.* Effect of varying amino acid levels on protein metabolism in nephrotic rats during total parenteral nutrition. *J Am Soc Nephrol* 1997; **8**: 1399–1404.
50. Derr RF, Alexander CS, Nagasawa HT. Metabolism of puromycin aminonucleoside in the normal, 'pre-nephrotic,' and nephrotic rat. *Proc Soc Exp Biol Med* 1967; **125**: 248–252.
51. Soares-da-Silva P, Fernandes MH, Pestana M. Studies on the role of sodium on the synthesis of dopamine in the rat kidney. *J Pharmacol Exp Ther* 1993; **264**: 406–414.
52. Adler CP. Relationship between deoxyribonucleic acid content and nucleoli in human heart muscle cells and estimation of cell number during cardiac growth and hyperfunction. *Recent Adv Stud Cardiac Struct Metab* 1975; **8**: 373–386.
53. Murotsuki J, Challis JR, Han VK *et al.* Chronic fetal placental embolization and hypoxemia cause hypertension and myocardial hypertrophy in fetal sheep. *Am J Physiol* 1997; **272**: R201–R207.
54. Gillebert TC, Leite-Moreira AF, De Hert SG. Load dependent diastolic dysfunction in heart failure. *Heart Fail Rev* 2000; **5**: 345–355.